Overcoming Oxygen Transfer Limitations with the Aachen™ High Shear Reactor

R Weideman[a*]

[a]*Maelgwyn Mineral Services Africa, Johannesburg 2188, South Africa*
**Corresponding author: reinhardt@maelgwynafrica.com*

ABSTRACT

Oxygen plays a critical role in gold cyanidation, directly influencing leaching kinetics and gold recovery. Conventional sparging often yields low volumetric mass transfer coefficients (k_La), limiting oxygen availability, particularly in ores containing oxygen consuming minerals. To address this, Aachen™ High Shear Reactors have been integrated into leaching circuits to enhance gas-liquid transfer through intensified turbulence and fine bubble dispersion. An empirical model was developed and validated to predict k_La in a leach tank equipped with an REA 030 Aachen™ reactor. Batch tests were conducted at a 2100 L scale using water and a 40% (m/m) silica flour slurry across three oxygen flow rates. Transient dissolved oxygen data were used to determine k_La, with performance benchmarked against ring and 0.5 µm frit spargers. The Aachen™ reactor achieved a maximum oxygen transfer efficiency of 91.7%, nearly double that of the frit sparger. A maximum standard oxygen transfer rate of 118 g/m³/h was obtained, with a saturation concentration of 38 mg/L at 20°C. The model showed strong predictive performance, with mean absolute percentage errors below 2% for both water and slurry systems. Continuous operation with silica slurry and sodium sulfite dosing confirmed the robustness of the approach under highly reactive conditions (~25 to 60 g/m³/h oxygen consumption load), with predicted apparent saturation concentrations agreeing with measured values within 1.86%. Under high oxygen demand, the Aachen™ reactor maintained dissolved oxygen concentrations above 20 mg/L at gas flow rates where conventional sparging systems became oxygen limited. The model enables reliable estimation of oxygen requirements and optimisation of delivery strategies, supporting improved oxygen utilisation and metallurgical performance.

Keywords: Gold, Oxygen, Shear, Oxidation, k_La

Introduction

Gold ore processing remains dominated by cyanidation, in which cyanide dissolves gold from crushed ore. The well-known Elsner equation describes the fundamental stoichiometric requirements for gold dissolution as shown in Eq. (1)

$$4Au + 8CN^- + O_2 + 2H_2O \rightarrow 4Au(CN)_2^- + 4OH^- \quad (1)$$

Although cyanide acts as the lixiviant, the oxygen demand predicted by this primary reaction is seldom sufficient in practice. Gold-bearing ores typically exhibit complex mineralogy, which promotes numerous competing side reactions consuming both oxygen and cyanide. In systems where gold is poorly exposed to the leaching solution, oxygen demand increases markedly. Oxygen demand is particularly evident in ores containing rapidly oxidising sulfide minerals such as pyrrhotite, or where gold is encapsulated within pyrite or arsenopyrite matrices (Rabieh *et al*., 2017)

Tailings reclamation circuits present a similar challenge. Here, unstable oxidation products, such as ferrous iron and metastable sulfide species, further increase reagent consumption. For this reason, effective pre-oxidation is often essential to control cyanide and oxygen demand and to stabilise overall leaching performance (Lotz *et al*., 2015).

In gas injection systems, the limitation is frequently not the reaction kinetics but gas-liquid mass transfer. If oxygen transfer into the slurry is insufficient, dissolved oxygen (DO) at the mineral surface becomes rate-limiting. The Aachen™ High Shear Reactor has been widely adopted in the gold processing industry to address high oxygen demand under such conditions. The reactor enhances oxygen dissolution within the slurry and applies intense shear forces, thereby improving gas dispersion and promoting favourable reaction kinetics for precious metal recovery (Flatman *et al*., 2015; Lotz *et al*., 2015). In tailings reprocessing operations, increased throughput rates further amplify oxygen requirements. The high oxygen transfer efficiency of the Aachen™ reactor allows the required oxygen to be delivered with lower overall gas consumption than conventional oxygenation systems (Botes, 2024).

Gas-liquid mass transfer

The transfer of oxygen from the gas phase into the liquid phase follows Fick's law of diffusion and is described as a liquid-film-controlled process (Kumar, 1991). In the bulk liquid, mixing and turbulence reduce concentration gradients. As a result, molecular diffusion is largely confined to a thin boundary layer at the gas-liquid interface (Mueller *et al.*, 2002). The corresponding mass flux, J, as shown in Eq. (2), can therefore be expressed as a function of the measurable concentration driving force and the empirically determined liquid film mass transfer coefficient, k_L

$$J = k_L (C^* - C) \quad (2)$$

When the interfacial area (A) per unit volume (V) is incorporated, the expression can be

reformulated in terms of the rate of change of the bulk phase concentration, as shown in Eq. (3).

$$J\frac{A}{V} = \frac{dC}{dt} = k_L a\,(C^* - C) \tag{3}$$

Here, C^*, denotes the saturation concentration of oxygen corresponding to the partial pressure of oxygen in the bulk gas phase. It is generally assumed to equal the concentration at the gas–liquid interface, since the resistance to mass transfer in the gas phase is negligible relative to that in the liquid phase, resulting in an insignificant concentration gradient on the gas side.

Temperature has an important influence on gas–liquid oxygen transfer as it affects both the equilibrium solubility of oxygen and the volumetric mass transfer coefficient. According to Henry's law, the equilibrium concentration of a dissolved gas is proportional to its partial pressure in the gas phase, with the corresponding Henry's law constant being temperature dependent (Sander, 2023). For oxygen in water, increasing temperature results in a decrease in equilibrium oxygen solubility (Benson and Krause, 1984). Consequently, differences in operating temperature need to be considered when comparing oxygen transfer measurements obtained under different experimental conditions.

The volumetric mass transfer coefficient, k_La, combines the liquid film mass transfer coefficient, k_L, and the specific interfacial area, a, available for gas–liquid exchange per unit volume. In practice, separating. k_L and a is rarely feasible. For this reason, these parameters are treated as a single measurable parameter that reflects the overall mass transfer performance in aerated systems.

Experimentally, k_La is most often determined from using dynamic DO measurements. The non steady state method is widely used for this purpose. In this approach, DO is first removed from the liquid, aeration is then initiated, and the subsequent reoxygenation profile is recorded. Analysis of the transient response allows estimation of the oxygen transfer characteristics and associated mass transfer parameters (Mueller *et al*., 2002).

In gold leaching systems, DO is simultaneously consumed through a series of oxidative reactions. This consumption is typically expressed as the oxygen uptake rate (OUR). Incorporation of the OUR into the transient mass balance yields Eq. (4).

$$\frac{\partial C}{\partial t} = k_L a\,(C^* - C) - OUR \tag{4}$$

Determining the OUR of the system requires a similar dynamic approach to that applied to k_La determination as the decay profile is inherently non-linear. The OUR can be described by Eq. (5), where k_{OUR} represents the decay rate constant and C_{Lim} denotes the asymptotic DO concentration approached during decay.

$$\frac{\partial OUR}{\partial t} = -k_{OUR}(C - C_{Lim}) \tag{5}$$

Substituting Eq. (5) into Eq. (4) yields Eq. (6), which enables the determination of k_La in systems where oxygen is simultaneously transferred and consumed within the liquid phase. This formulation

accounts for the presence of an active oxygen consumer, thereby providing a more realistic representation of mass transfer under reactive conditions.

$$\frac{\partial C}{\partial t} = -k_{OUR}(C - C_{Lim}) + k_L a\,(C^* - C) \quad (6)$$

Empirical correlations commonly relate $k_L a$ to the specific power input, and superficial gas velocity, u_{sg}, as expressed in Eq. (7).

$$k_L a = K\ u_{sg}^{\alpha}\ \left(\frac{P}{V}\right)^{b} \quad (7)$$

This power density model reflects the combined effects of turbulence generation and gas throughput. Increasing power input enhances energy dissipation and reduces boundary-layer thickness, while higher gas velocities increase interfacial area and promote bubble renewal, both of which contribute to improved oxygen transfer. These relationships, described in texts such as Principles of Fermentation Technology (Stanbury *et al*., 2013.), form the basis for predicting and optimising oxygen transfer during scale-up and industrial operation.

In this paper, however, specific power was replaced by solution pressure as the primary hydrodynamic descriptor. Solution pressure provided a more direct and scalable measure of energy dissipation under high-shear conditions, where mechanical power measurement is less practical.

Materials and Methods

Equipment

The DO was measured using a YSI ProODO optical meter. Oxygen flow was controlled with a Bronkhorst FlexiFlow FFAJK20L mass flow controller.

Aachen™ reactor performance was compared to conventional sparging using two configurations: a ring sparger and a 0.5 µm frit sparger (Figure 1). The frit sparger served as a high efficiency benchmark for gas dispersion.



Figure 1. Ring and 0.5 µm frit spargers.

Experimental configuration

To evaluate the Aachen™ reactor under conditions representative of industrial-scale operation, the REA 030 reactor was integrated with a 2100 L agitated tank. Recirculation was achieved using a WEIR Warman 1.5/1 centrifugal pump of the same scaled configuration as that used in industrial installations, as shown in Figure 2. Tests were conducted using both water and slurry. The slurry consisted of 150-mesh-screened silica flour, at a solids concentration of 40% by mass.

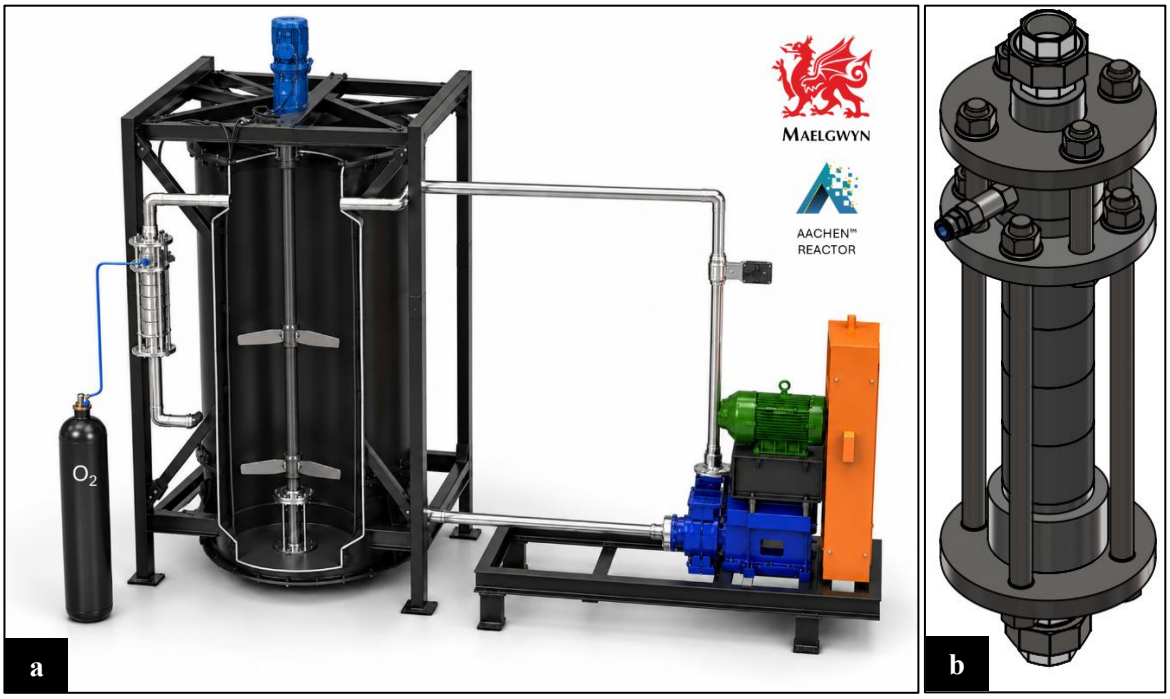


Figure 2. (a) - 2100 L pilot scale Aachen™ REA 030 test layout, (b) – Aachen™ REA 030.

Experimental conditions and procedures

Experimental procedures were designed to replicate oxygen flow rates, along with solution flow rates and pressures, representative of industrial operation. Obtaining sufficient data for fitting the power density model (Eq. (7)), several tests were conducted over a range of slurry pressures and oxygen flow rates. Three oxygen flow rates were selected based on the equivalent oxygen to slurry ratio of an industrial Aachen™ reactor (REA 450) operating at a slurry throughput of 700 m^3/h. The corresponding equivalent oxygen flow rates for the REA 030, expressed in normal litres per minute (NL/min), are summarised in Table I.

Table I. REA 450 vs REA 030 flow at scale determination.

REA 450 (O_2 flow kg/h)	REA 030 (O_2 flow NL/min)
159	5.5
100	3.5
43	1.5

Validation of the Aachen™ system at pilot scale required steady-state continuous operation under the conditions summarised in Table II, corresponding to a 1:1 representation of an industrial pre-oxidation circuit. Sodium sulfite was continuously dosed using a Watson Marlow Qdos dosing pump to simulate oxygen consumption by a reactive ore, with the dosage adjusted to achieve varying consumption rates. Cobaltous sulfate was added at a concentration of 1 mg/L to catalyse the sulfite oxidation reactions.

Table II. Process conditions of a continuously operated system.

Parameter	Value	Unit
Tank volume	1750	L
Feed slurry flow rate	875	L/h
Tank residence time	2	hrs
Oxygen supply rate	6	NL/min
Aachen™ slurry pressure	4	Bar
Aachen™ slurry flow rate	2100	L/h
Aachen™ passes (Aachen flow / Feed flow)	2.4	-

Modelling workflow procedures

All data processing, modelling, and visualisation were performed using the WinPython 64-bit distribution (Python 3.13.1 environment). Analysis focused on parameter estimation, numerical integration of differential equations, statistical evaluation, and graphical representation of experimental results. The principal Python libraries utilised in this study are summarised in Table III.

Table III. Primary Python packages used for data analysis and modelling.

Package	Primary function
NumPy	Numerical array operations and mathematical computations
SciPy	Non-linear regression, optimisation, numerical integration, and signal processing
Pandas	Data handling and structured dataset manipulation
Matplotlib	Data visualisation and figure generation
Scikit-learn	Statistical metrics, including the coefficient of determination

The experimental data was used to solve the differential equations presented in Eq. (4), (6), and (7) to obtain the fitted parameters $k_L a$ and C^* for the system. Parameter estimation was performed by fitting the model predictions to the measured DO profiles. The resulting experimental dataset was further subjected to multiple regression analysis to determine the empirical constants in Eq. (7), relating $k_L a$ to the specific solution pressure and superficial gas velocity.

Results and discussion

Temperature normalisation of oxygen transfer data

The water and slurry experiments were conducted over a relatively narrow temperature range of

22.3–32.3°C, with the increase in temperature primarily attributed to shear within the system. To enable direct comparison between tests, all experimentally determined k_La and C^* values were normalised to 20°C. Repeat tests conducted under comparable hydrodynamic and oxygen supply conditions produced similar oxygen transfer rates across this temperature range. The oxygen transfer rate was therefore assumed to remain effectively constant over the investigated range and was used as the basis for normalising the fitted parameters to 20°C.

Batch experimental results

The water and slurry test campaigns produced 18 and 14 experimental k_La datapoints respectively. These datasets were used to estimate the parameters in Eq. (7), and the resulting correlations are shown in Figure 3.

The fitted models yielded mean absolute percentage errors (MAPEs) of 1.18% for the water system and 0.85% for the slurry system. All datapoints were predicted within ±2.81% (water) and ±2.17% (slurry) of the measured values. This level of accuracy indicates very close agreement between experimental measurements and the proposed model.

The fitted parameters for Eq. (7) were similar across both media, indicating that the underlying hydrodynamic behaviour of the Aachen™ reactor is largely preserved when transitioning from water to slurry. Although suspended solids introduce additional complexity, the dominant mass transfer mechanisms appear to remain unchanged. This supports the applicability of the proposed correlation under both single- and multiphase conditions.

Figure 4 compares the oxygen transfer performance of the Aachen™ reactor with that of a conventional sparging system in both water and slurry. At low oxygen flow rates, the Aachen™ transfer efficiencies approached 90%, while values of approximately 65% were obtained at the nominal flow rate, representing an improvement of roughly 20% over conventional sparging.

With increasing gas flow, the efficiency gap narrowed to roughly 10%. Despite this, the Aachen™ system maintained a higher oxygen transfer rate, reaching 118 g/m³/h compared with 98 g/m³/h for the sparger. In practice, any reduction in efficiency at higher gas throughput can be mitigated by installing additional reactor units to maintain overall oxygen transfer performance and process stability.

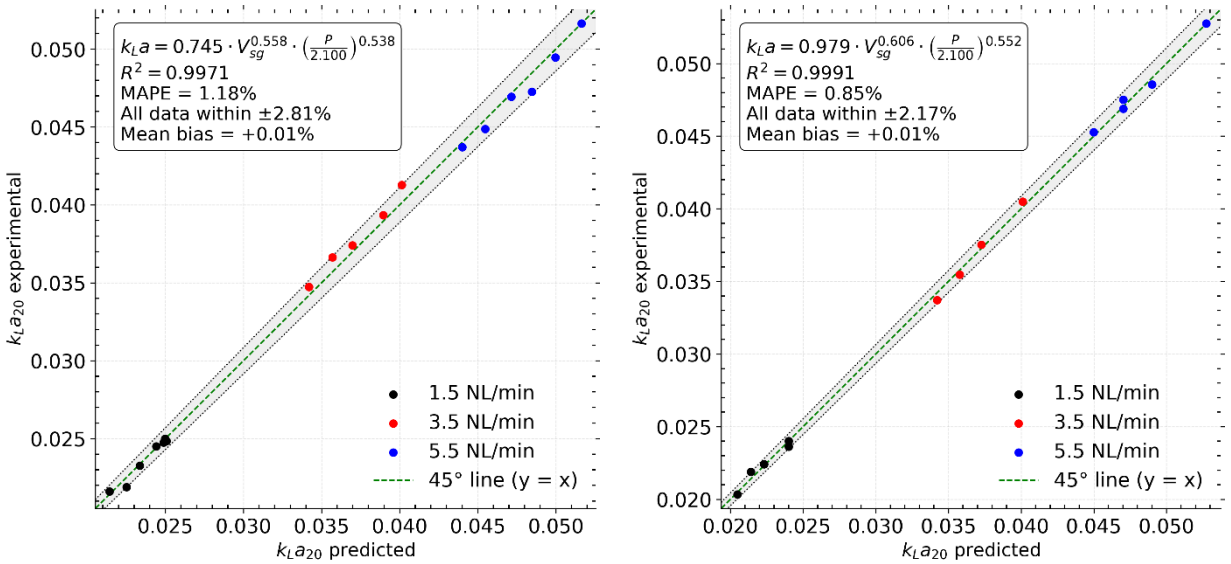


Figure 3. Comparison of experimentally determined and model-predicted k_La_{20} values for the 2100 L pilot scale tests under water (left) and slurry (right) conditions.

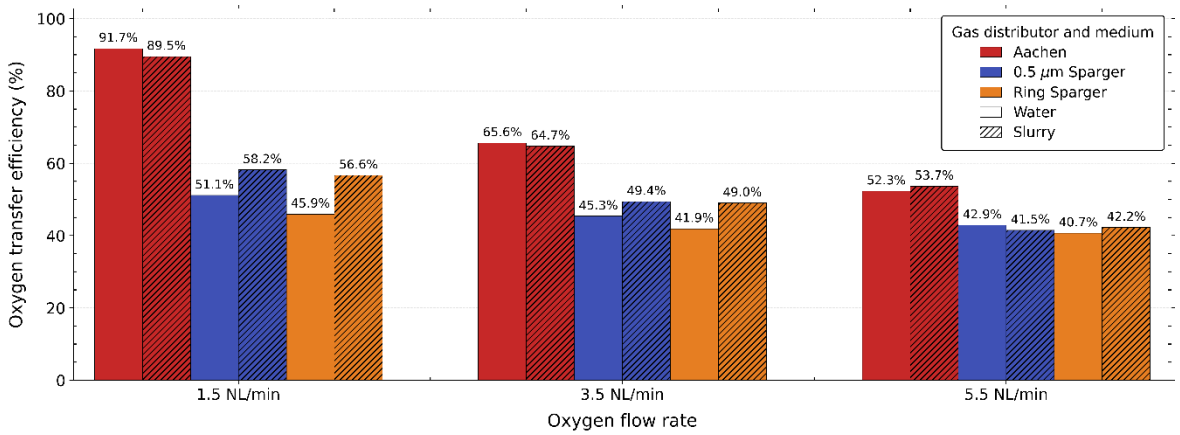


Figure 4. Comparison of oxygen transfer efficiencies between the Aachen™ reactor and conventional sparging configurations for water and slurry systems.

Continuous experimental results

Performance Comparison under High Oxygen Uptake Conditions

System performance under high oxygen demand was evaluated using a slurry simulating a highly oxygen-consuming ore. The slurry was continuously fed at a rate equivalent to 50% of the oxygen transfer capacity under the selected operating conditions, thereby imposing a controlled and sustained OUR. This approach allowed direct comparison between the Aachen™ reactor and a conventional 0.5 µm frit sparger. The resulting continuous operation profiles are presented in Figure 5.

The green region represents continuous slurry operation with sodium sulfite dosing in the absence of oxygen supply. Under these conditions, DO decreased steadily, confirming the severity of oxygen demand.

Operation with the Aachen™ reactor is shown by the red trace during continuous slurry and sodium sulfite dosing. DO concentrations above 20 mg/L were achieved, demonstrating the reactor's

ability to overcome the imposed oxygen demand and sustain non-limiting conditions.

Subsequently, both the Aachen™ reactor and the sodium sulfite feed were stopped, and the oxygen supply was switched to the 0.5 µm frit sparger, as indicated by the blue trace. The sodium sulfite feed was then reintroduced immediately after the oxygen addition resumed. DO concentrations declined rapidly, indicating that at the same oxygen flow rate, the sparger was unable to meet the imposed OUR and oxygen-limited conditions developed. In an industrial leaching circuit, sustained oxygen limitation of this nature would be expected to reduce dissolution kinetics and, ultimately, overall gold recovery.

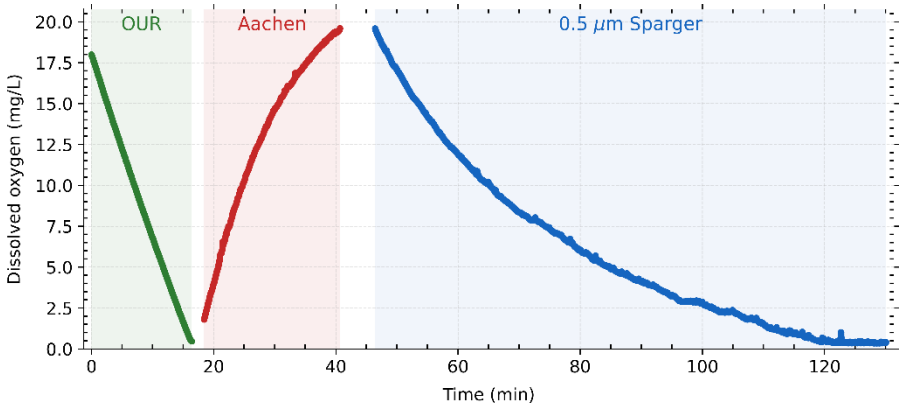


Figure 5. Comparison of oxygen transfer capabilities between the Aachen™ reactor and conventional oxygenation devices.

Determination of k_La under continuous slurry operation with oxygen uptake

The applicability of Eq. (6) for estimating k_La under continuous oxygen-consuming conditions was assessed by dosing sodium sulfite (Na_2SO_3) at varying rates, corresponding to an oxygen consumption load of approximately 25 to 60 g/m³/h during continuous slurry operation. This approach allowed evaluation of the model under reactive conditions, where the presence of an oxygen consumer is expected to influence the apparent saturation concentration and reduce the observed oxygen transfer rate. Such conditions provide a more rigorous test of the model formulation.

Figure 6 presents the steady state DO concentrations measured at different sodium sulfite dosages. Increasing the imposed OUR led to a progressive decrease in the steady state DO concentration. This behaviour reflects the coupling between oxygen transfer and consumption under reactive conditions and supports the validity of the extended mass balance framework described in Eq. (6).

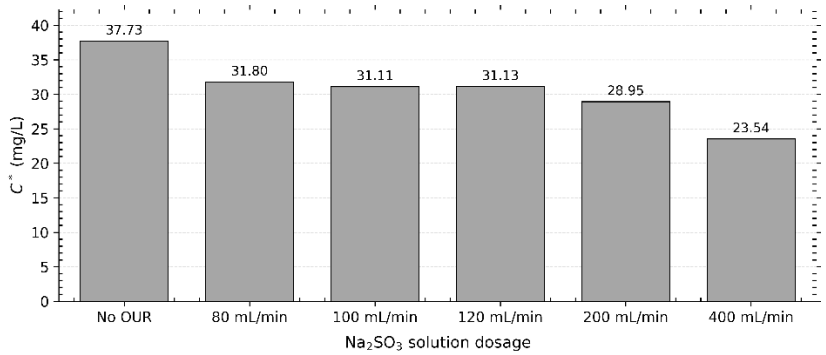


Figure 6. Apparent oxygen saturation concentrations under varying sodium sulfite dosages simulating oxygen consumers in solution.

Figure 7 presents the predicted k_La values and oxygen transfer efficiencies across the range of sodium sulfite dosages. The fitted k_La values showed low variability, with a coefficient of variation of 4%, a mean of 0.0739 min^{-1}, and a standard deviation of 0.0030 min^{-1}. The experimentally-determined oxygen transfer efficiencies exhibited similar consistency. Under baseline conditions, an efficiency of 57.87% was obtained, while the OUR test conditions deviated by no more than 5 percentage points. The standard deviation across these tests was 1.52%, with a mean average percentage error of 2.64%.

Overall, these results demonstrate that the proposed approach, based on Eq. (6), provides reliable estimates of k_La and oxygen transfer efficiency in the presence of an oxygen consumer.

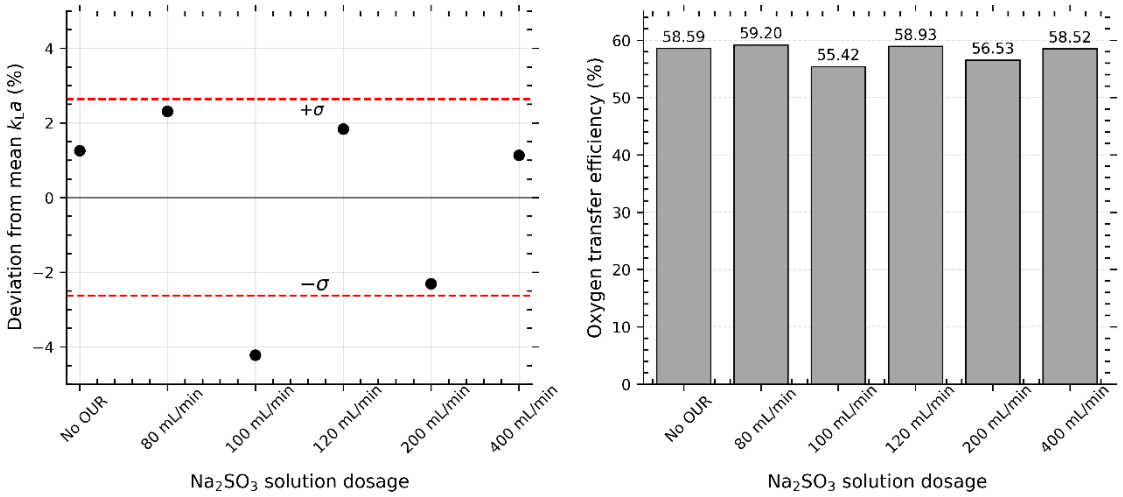


Figure 7. Predicted k_La and oxygen transfer efficiencies under varying sodium sulfite dosages simulating oxygen consumers in solution.

Validation of apparent saturation concentration under reactive conditions

Under state conditions, the accumulation term in Eq. (7) becomes zero ($\frac{\partial C}{\partial t} = 0$), such that the rate of oxygen transfer into the liquid equals the OUR. Substituting and rearrangement of Eq. (7) yield the steady state relationship given in Eq. (8):

$$C_{app}^{*} = \frac{k_L a\, C^{*} + k_{OUR}\, C_{Lim}}{k_L a + k_{OUR}} \tag{8}$$

This expression indicates that, in the presence of an oxygen consumer, the observed steady state concentration reflects a balance between the intrinsic saturation concentration and the asymptotic concentration associated with oxygen uptake kinetics.

Figure 8 compares the predicted apparent saturation concentrations with corresponding experimental measurements. Predictions were based on the baseline k_La obtained under non-reactive conditions, together with independently determined k_{OUR} and C_{Lim} values. Close agreement between predicted and measured concentrations was observed, with a MAPE of 1.86%, and a mean absolute deviation of 0.637 mg/L. These results indicate that the steady state formulation provides reliable predictions under reactive slurry conditions.

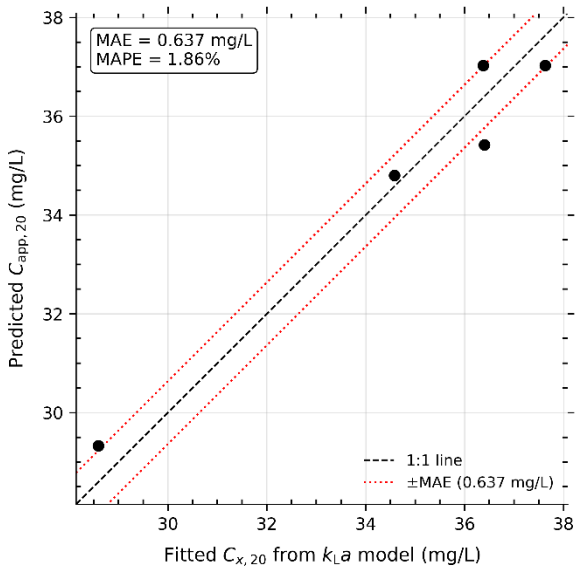


Figure 8. Apparent oxygen saturation concentrations under varying sodium sulfite dosages simulating oxygen consumers in solution.

Conclusions

Oxygen transfer remains a key limitation in high demand cyanidation systems. The present study shows that the Aachen™ High Shear Reactor mitigates conventional gas–liquid mass transfer constraints through intensified shear and improved gas dispersion.

Performance was consistently superior to conventional sparging where the oxygen transfer efficiency of up to 90% at the pilot scale was achieved. At higher gas throughput levels, the Aachen™ system continued to deliver higher oxygen transfer rates, reaching 118 g/m³/h compared with 98 g/m³/h for sparging.

The extended mass balance, incorporating oxygen uptake kinetics, provided an accurate description of reactive slurry behaviour, with prediction errors below 2%. Under high oxygen demand, the Aachen™ reactor maintained DO above 20 mg/L at gas flow rates at which sparging became oxygen-limited.

Overall, the results demonstrate that the Aachen™ High Shear Reactor offers improved oxygen transfer performance and stable operation under reactive conditions. The validated modelling framework approach also provides a practical tool for optimising oxygen delivery and enhancing metallurgical performance in high oxygen demand gold processing circuits.

Acknowledgements

The author gratefully acknowledges Maelgwyn South Africa and Maelgwyn Mineral Services Africa for providing financial support and technical assistance in the execution of the testwork campaign.

References

Benson, B.B. and Krause, D., Jr., 1984. The concentration and isotopic fractionation of oxygen dissolved in freshwater and seawater in equilibrium with the atmosphere. Limnol. Oceanogr., 29(3), 620–632.

Botes, W.J., 2024. The benefits of using the Aachen high shear reactor in gold tailings reprocessing: From laboratory to plant evaluations. In: Proceedings of the Hydrometallurgy for the future, Western Cape, South Africa. pp. 15-24.

Flatman, S., Battersby, M., Lotz, P., and Sprenger, H., 2015. Twenty years of development to commercial demonstration of the Aachen Reactor™. In: Proceedings of Precious Metals '15, UK.

Kumar, R., 1991. Oxygen transfer by mechanical aeration. M.E thesis, Dept. of Civil Engineering, University of Rurkee, India.

Lotz, P., Van der Merwe, J., Mogashoa, S., Flatman, S. and Imhof, R., 2015. Aachen Reactors™, a proven system to realise hidden economic potentials. In: Proceedings of The Southern African Institute of Mining and Metallurgy World Gold Conference, South Africa.

Mueller, J., Boyle, W.C. and Popel, H.J., 2002. Aeration: Principles and Practice, Volume 11. CRC Press, USA.

Rabieh, A., Eksteen, J.J. and Albijanic, B., 2017. The effect of grinding chemistry on cyanide leaching of gold in the presence of pyrrhotite. Hydrometallurgy, 173, pp.115-124.

Sander, R., 2023. Compilation of Henry's law constants (version 5.0.0) for water as solvent. Atmos. Chem. Phys., 23, 10901–12440.

Stanbury, P.F., Whitaker, A. and Hall, S.J., 2013. Principles of fermentation technology. Elsevier. Netherlands, 2nd edition.

Thakre, S.B., Bhuyar, L.B. and Deshmukh, S.J., 2008. Effect of different configurations of mechanical aerators on oxygen transfer and aeration efficiency with respect to power consumption. Int. J. Aerosp. Mech. Eng., 2(2), 100–108.